In-situ Scrutiny of the Relationship between Polymorphic Phases and Properties of Self-Assembled Monolayers of a Biphenyl Based Thiol

Markos Paradinas,[a,‡] *Carmen Munuera,*[a,§] *Manfred Buck*[b] *and Carmen Ocal*[a*]

[a] Institut de Ciència de Materials de Barcelona (ICMAB-CSIC), Campus UAB, Bellaterra 08193-Barcelona, Spain

[b] EaStCHEM School of Chemistry, University of St. Andrews, North Haugh, St. Andrews, KY169ST, UK

ABSTRACT. Two polymorphic phases of ω-(4'-methylbiphenyl-4-yl) butane-1-thiol (BP4) molecules formed on Au(111) were investigated by multi-dimensional atomic force microscopy, combining conductivity measurements, electrostatic characterization, friction force mapping and normal force spectroscopy. Based on the same molecular structure but differing in molecular order, packing density and molecular tilt, the two phases serve as a test bench to establish the structure-property relationships in self-assembled monolayers (SAMs). From a detailed analysis of the charge transport and electrostatics the contributions of geometrical and electronic effects to the tunneling are discussed.

INTRODUCTION

Conceptualizing the transport characteristics of molecules bonded between metal electrodes is of fundamental importance for molecular scale electronics. Both theoretical and experimental studies have established that the systems' properties are determined by a complex interplay of factors comprising the intrinsic properties of molecules, their supramolecular arrangement, and geometry and chemistry of the contacts between molecule and electrode.[1–6] While the field has advanced to the single molecule level,[7,8] the challenges associated with the generation of reliable single molecule devices[9] make nanoscopic ensembles of molecules a more likely scenario for technological exploitation. From this point of view self-assembled monolayers (SAMs) are attractive systems,[10,11,12] owing to the versatility of designing and manipulating their structure, chemical functionality and electronic properties by appropriate choice of the molecular building blocks. For instance, modification of the work function of electrodes by SAMs altering the interfacial dipole is one of the methods employed to reduce the injection barrier in organic electronic devices. [13,14] Exemplifying the role of SAMs for controlling interfacial properties, this is accomplished by tailoring of the molecular structure.[15,16] However, alterations at the molecular level are also likely to affect the molecular packing which, from a fundamental point of view, raises the question of how much a change in the arrangement of the molecules contributes to the overall change in the property of a SAM. To address this point, access to different structures without altering the molecular architecture is required and this has been exploited in studies establishing the influence of molecular packing on mechanical/tribological properties[4,17] and charge transport[18,19] in alkanethiol SAMs. Similarly, aromatic SAMs have been investigated.[20–23] Compared to the archetypal alkanethiol SAMs, layers based on aromatic molecules display a

range of properties of interest for potential applications, such as their behavior towards electron radiation[24–26] and charge transfer processes,[27–29] which make them attractive for molecular electronics and electrode modification.[30,31] A specific type of aromatic thiol SAM, featuring a combination of an aromatic unit with a short alkane spacer,[32–35] is of particular interest as regards the understanding of the above mentioned influence of the molecular packing on film properties. SAMs of thiols combining a biphenyl moiety with an even-numbered alkane chain have been shown to exhibit polymorphism on Au(111),[36,37] thus enabling to scrutinize the influence of the supramolecular arrangement on different surface properties. In addition, the selected system of ω-(4'-methylbiphenyl-4-yl) butane-1-thiol (BP4) has also been employed to shed light onto an equally important question related to the inherent limit of scanning tunneling microscopy (STM) to accurately determine sub-nanometric topographic differences between molecular phases coexisting in organic thin films. Contrasting STM, in which surface topography and density of states (DOS) are convoluted, conductive atomic force microscope (C-AFM) can be employed to provide simultaneous measurements of topography and conductive response of the film.

A combined strategy, in which conventional C-AFM is complemented by spectroscopic measurements, is presented as a reliable means to determine the relationship between structure and electronic properties of self-assembled monolayers. Besides reconciling topographic and electronic characteristics, the local work function obtained by Kelvin probe force microscopy (KPFM) helps analyzing the role played by the molecular dipoles.

EXPERIMENTAL

Self-assembled monolayers of BP4 on gold were prepared as previously detailed.[32,36,38] Gold films, 300 nm thick, evaporated onto mica were used as substrates (Georg Albert PVD, Germany). To obtain large and atomically flat (111)-oriented terraces, the substrates were flame annealed in air. Complete monolayers exhibiting exclusively the low-temperature α-phase were prepared by immersing the substrate in a 0.1–1 mM solution of BP4 in ethanol at 338 K for 12–24 h. It is noted that neither concentration nor immersion time is critical for the preparation.[36] The transition to the high-temperature β-phase is induced by post annealing the α-phase sample at 373 K in a nitrogen atmosphere.[36] Coexistence of the two phases is achieved by annealing the sample for about 15–18 h. The ratio between areas covered by each phase can be adjusted by varying the annealing time. The structure of these two molecular phases (see below) has been reported in detail.[36,37]

A commercial head from Nanotec Electronica was used for atomic force microscopy (AFM) measurements which were performed in an N_2 environment (RH ≈ 2%) to eliminate humidity effects. All data were analyzed using the WSxM freeware.[39] Samples were comprehensively characterized by acquiring topography, friction, conductivity and electrostatic data from exactly the same locations. To exclude any induced surface modification, AFM images were acquired in a non-invasive manner by using either the contact operation mode at the lowest possible applied load (attractive regime close to the pull off force) or the non-contact regime during dynamic measurements. Thus, the pull off contact mode was employed in topographic AFM, in friction force microscopy (FFM), as well as in conductive AFM (C-AFM) and the dynamic non-contact Kelvin probe force microscopy (KPFM) was used to measure the local contact potential difference (CPD) between tip and sample.

Depending on the specific experiment, tips of different materials mounted on cantilevers with the appropriate stiffness were employed: i) Si tips and low nominal force constant (k = 0.05 Nm^{-1}) cantilevers for FFM; ii) conducting Cr-Pt coated tips in cantilevers with nominal k = 0.2 Nm^{-1} and resonance frequency 13 kHz or k = 3 Nm^{-1} and resonance frequency 75 kHz for C-AFM or KPFM, respectively. The same tip was used in all the experiments of at least one set. The choice of cantilevers with appropriate stiffness enabled us to switch from contact to non-contact mode measurements, under controlled experimental conditions without changing surface location. Therefore, we obtained unambiguous correlation between topography, conductivity and electrostatic information of the structurally different phases existing side by side.

In addition to common imaging, the so-called three-dimensional (3D) mode was employed to combine conductivity and electrostatic characterization with force spectroscopy.[40,41] These modes are a convenient way for recording images $f_i(x_1, x_2)$ where fast (x_1) and slow (x_2) scan axis do not necessarily correspond to distances.[42,43] In particular, monitoring the normal force ($f_1 = F_n$) and current flow ($f_2 = I$) as a function of tip–sample voltage ($x_1 = V_{tip}$) and vertical piezo-displacement ($x_2 = z$), $F_n(V_{tip}, z)$ and $I(V_{tip}, z)$ images can be obtained at specific surface points. Starting at a distance above the surface, the tip is approached until contact. In this way, the electrostatics and conductivity together with the mechanical response of the sample are probed as a function of the piezo displacement. On the one hand, force versus distance (F-z) curves correspond to vertical line profiles in the $F_n(V_{tip}, z)$ image. On the other hand, at tip-sample distances prior to tip-sample contact, horizontal profiles in $F_n(V_{tip}, z)$ should present the parabolic curves corresponding to electrostatic interaction centered at the tip-sample CPD.

Horizontal line profiles on $I(V_{tip}, z)$ provide current versus voltage characteristics (I-V curves). These 3D operation modes offer the advantage of independent yet simultaneous data acquisition, thus minimizing time-dependent changes in the properties of sample or probes or any uncertainty in position, while maintaining a precise control over the applied load and the tip-sample distance.[40,44,45]

To derive the local work function, CPD values obtained by KPFM imaging were cross-checked by using the above described 3D mode in which the electrostatic force was measured at a given surface point as a function of the applied voltage.[41] In the employed geometry the voltage is applied to the tip and, as a consequence higher CPD values indicate lower work function (ϕ). More details on the experimental techniques are provided in the Supporting Information.

RESULTS AND DISCUSSION

Details on the two structural phases of BP4 on Au(111) have been investigated by different surface science techniques including STM.[37,38] They are described by a rectangular centered $5\sqrt{3}$ x3 (α-phase) and an oblique $6\sqrt{3}$ x$2\sqrt{3}$ (β-phase) unit cell. Both containing eight molecules their dimensions are 24.94 Å x 8.64 Å and 29.93 Å x 9.98 Å which correspond to an area per molecule of $A_\alpha = 27.05$ Å^2 and $A_\beta = 32.4$ Å^2, respectively. The estimated molecular tilt angles for each phase are $\varphi_\alpha \approx 40°$ and $\varphi_\beta \approx 45\text{-}49°$ with respect to the surface normal.[32,38] In principle, for a sample where both phases coexist, the difference in the film thickness between them might

be determined by STM. However, due to the inherent convolution of topography and electronic effects in STM, on surfaces with laterally heterogeneous DOS, the height difference measured by STM in constant current mode (cc-STM) may differ from the geometric value. This is pinpointed by comparison of data from ellipsometry and X-ray photoelectron spectroscopy (XPS) with STM data. For samples in which complete SAMs of only one of the phases exist (see Experimental), the spectroscopies yield values for the film thickness of $d_\alpha = 16.2 \pm 0.7$ Å and $d_\beta = 14.4 \pm 0.7$ Å, i.e., a height difference of $\Delta d = 1.8$ Å.[32,37,38] In comparison, the difference measured by cc-STM in samples where both phases coexist (see Figure S1 in Supporting Information) amounts to $\Delta h_{\alpha-\beta} = 0.8 \pm 0.2$ Å, which is considerably smaller than the spectroscopic value. Since one of the factors determining the apparent height measured by cc-STM is the work function, its local variations must be taken into account. In an attempt of reconciling results from different techniques, we investigate the influence of electronic effects by employing a combination of AFM modes which allow simultaneous measurements.

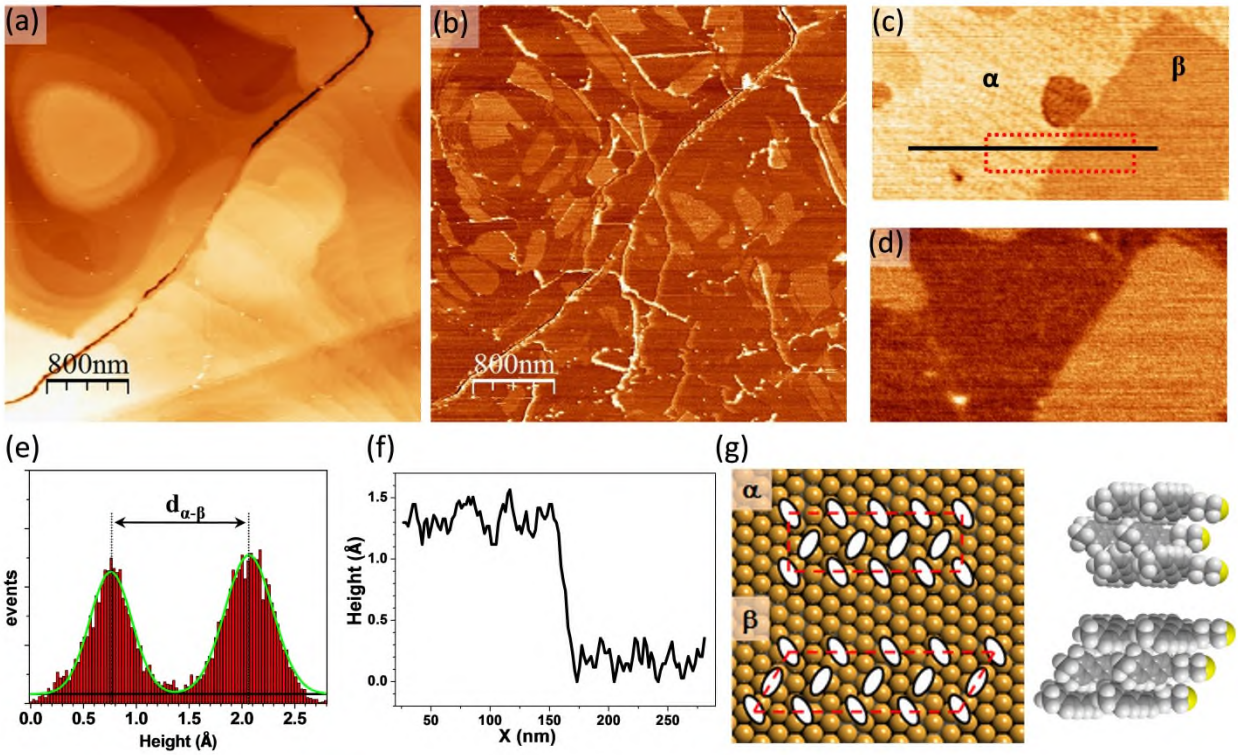

Figure 1. (a, c) Contact AFM topographic and (b, d) simultaneously measured lateral force (forward) images for a BP4 SAM on Au(111). z-scale in (a) is 18 nm and lateral dimensions in (c) are 400 nm x 215 nm. (e) Height histogram and (f) topographic profile corresponding to the red dashed rectangular area and the black segment indicated in (c) and (g) schematics of the two molecular packings.

Previous studies of the BP4 system,[22,23] combining high resolution and sensitive friction measurements, established a distinct difference in the tribological response of the α and β phases. This makes lateral force imaging a convenient method for their identification as illustrated by the large scale images of Figure 1 which show simultaneously measured topography and friction. The two phases are clearly distinguished in lateral force (Figure 1b) in contrast to topography (Figure 1a) where the large z range needed to follow the topography of

the substrate (hundreds of Ångstroms) masks the small height difference between α and β phases (below two Å). Therefore, throughout the present work, lateral force imaging was used to easily distinguish between the two phases and unambiguously correlate them with their properties. It is noted that, as seen from Figures 1c-d, the β-phase exhibits the higher friction.[22,23] The difference in thickness between the two phases was accurately determined from high magnification topographic images as displayed in Figure 1c. Evaluation of height histograms (Figure 1e) and line profiles (Figure 1f) yields a value of $\Delta d_{\alpha-\beta} = 1.2 \pm 0.2$ Å which is between the 1.8 Å and 0.8 Å derived from XPS[37] and cc-STM, and ascribed to the phase dependent molecular packing and orientation. Models of the two phases are shown in Figure 1g. The most important differences between the phases are the intermolecular distances, and the tilt and twist angles of the biphenyl moieties. Referring to previous work[37] for a detailed discussion, we note at this point that the depicted models reflect structures which are consistent with the STM and spectroscopic data[32,37] but cannot claim to reflect all details due to limitations in the interpretation of the experimental data. One important parameter in this regard is the twist angle of the aromatic moieties which, as known from experiment, differ substantially in the two phases. However, the exact nature of this difference is unclear as the experiments cannot identify the torsion between the rings of a biphenyl unit. While the models display the biphenyl units in the usually assumed coplanar conformation, this is likely to be oversimplified as DFT calculations on aromatic SAMs find some torsion.[46–49] Since the torsional angle affects the conductance[48,49] it is important to disentangle electronic and topographic contributions in order to fully understand the structural details of the SAMs and the apparent discrepancy between the topographic data from the different techniques. Therefore, assessing the phase dependent conductivity and work function by C-AFM and KPFM measurements is essential.

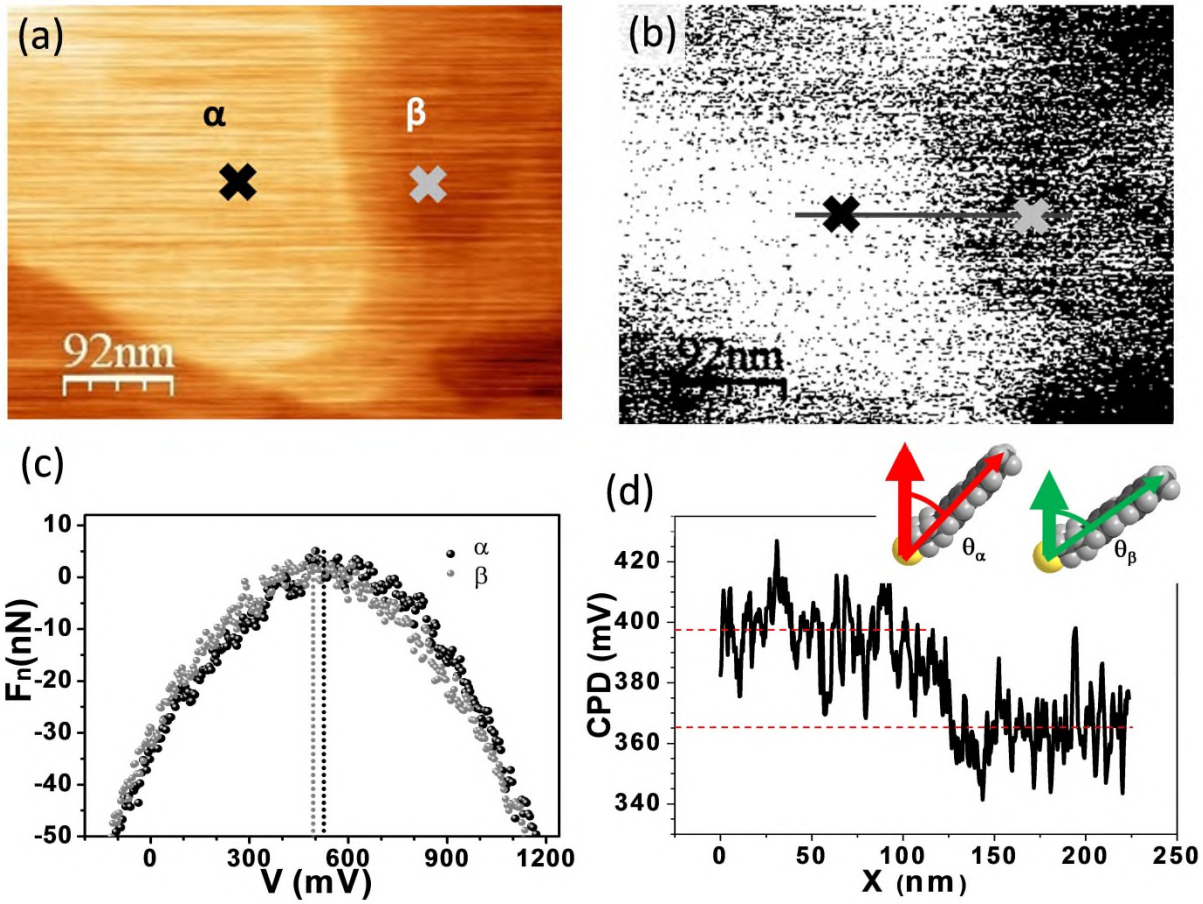

Figure 2. (a) Topographic image and (b) KPFM map of the same surface location.(c) Normal force versus bias voltage parabolas measured on the locations of the α (black) and β (gray) phases indicated in (a). (d) Contact potential difference profile taken along the line indicated in the KPFM map of (b). Inset: schematic representation of the molecular dipole for the two tilted configurations.

It is known that the same molecule can have different ionization potentials when it is isolated or part of an ordered supramolecular structure,[50] thus making the work function dependent on the

structural details of the molecular layer. As we have already demonstrated for both organic and inorganic laterally heterogeneous surfaces,[41,51,52] CPD measurements provide a map of the work function change independent of the tip material (see also Supporting Information). Results for the mixed phase BP4 SAM are shown in Figure 2. Comparison between Figure 2a and 2b indicates that the thicker α-phase ($d_\alpha > d_\beta$) is associated with regions of lower work function ($\phi_\alpha < \phi_\beta$). The difference in CPD values between the α and β phases is $\Delta CPD_{\alpha\beta} \approx$ 30-40 mV either by direct measurement of force versus voltage $F_n(V)$ curves at specific surface locations (Figure 2c) or by KPFM mapping (Figure 2d). These results were verified by cross-checking measurements including topographic, FFM and CPD data on diverse surface regions (Figure S2 in the Supporting Information).

Commonly, the measured change in CPD is ascribed to a change in the work function introduced by a surface layer of point dipoles. Within the classical electrostatics approach this is described by the Helmholtz equation:[53]

$$\Delta\phi = -\frac{\mu_z}{\varepsilon_0 A} \qquad (1)$$

where ε_0 is the vacuum permittivity, μ_z is the normal component of the dipole of one individual molecule within the layer and A is the surface area occupied by the molecule. Unexpectedly low work function changes have been successfully described by introducing an effective dielectric constant, ε_{eff}, in the Helmholtz equation which resolves the shortcomings of the point dipole approximation.[54] The effective dielectric constant of the monolayer material would also account for the reduced molecular dipole in densely packed layers. Accordingly, the difference in work function between regions covered by the two BP4 phases can be described by:

$$\Delta\phi_{\alpha\beta} = \frac{\mu_\alpha}{\varepsilon_0 \varepsilon_\alpha{}^{eff} A_\alpha} - \frac{\mu_\beta}{\varepsilon_0 \varepsilon_\beta{}^{eff} A_\beta} \qquad (2)$$

where the subscripts indicate correspondingly the α and β phases. That is, $\Delta\phi_{\alpha\beta}$ is determined by a combination of parameters comprising packing density, static dipole moment, and the molecular polarizability expressed by the effective dielectric constant, all of which are dependent on the orientation of the molecules. Deconvolution of all this factors by detailed modeling and electrostatic calculations being out of the scope of the present work, we take a phenomenological approach and investigate by phase dependent conductivity measurements how all contributions together affect the conductance of the layers.

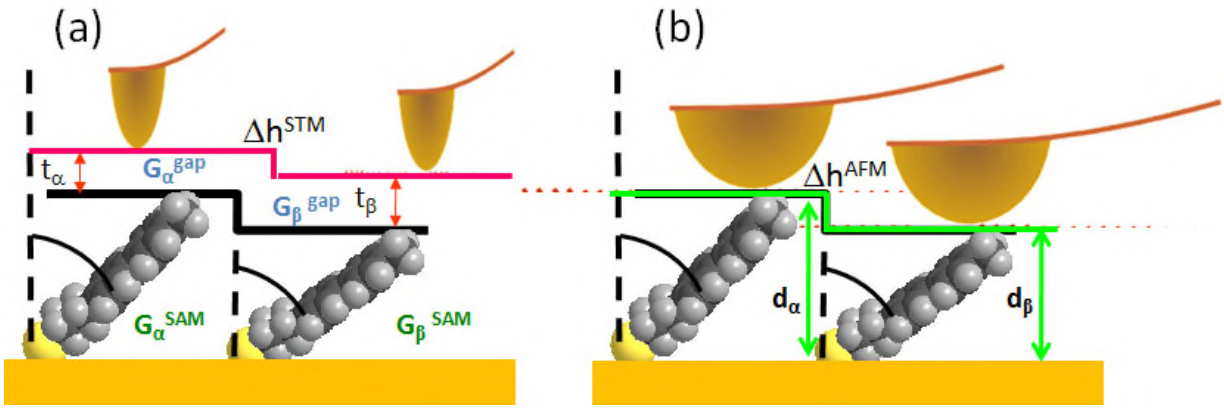

Figure 3. (a) Two-layer tunnel junction model in cc-STM with t_α and t_β denoting the vacuum barrier widths on the corresponding phases of the BP4 SAM. (b) Schematics of thickness difference measurements by contact AFM.

Assessing conductance in laterally heterogeneous SAMs by cc-STM, the obtained topographic image is described within the two-layer tunnel junction barrier model [55] sketched in Figure 3a

(for explanation of the two-barrier model for conductance through SAMs see Supporting Information), and the electron tunneling between the STM tip and the Au(111) substrate is defined by the product of the SAM and vacuum gap conductances ($G = G^{gap}\ G^{SAM}$). In comparison, C-AFM (Figure 3b) eliminates the vacuum gap and the difference in thickness obtained by the two techniques can, in principle, be estimated from the difference in barrier width for each one of the BP4 phases $\Delta h_{STM} = \Delta h_{AFM} + \Delta t$. As shown later on, $\Delta t = t_\beta - t_\alpha$ can be deduced if transport across the layers is determined by specially designed C-AFM experiments presented next.

Local current versus voltage characteristics (I-V curves) were obtained for both polymorphic phases of the BP4 layer by employing the 3D mode described above. The AFM tip was located at specific points (scan disabled) on top of the α and β phases, avoiding gold grain boundaries and defects within the monolayer. By combining the information from the simultaneously acquired $F_n(V, z)$ and $I(V, z)$ images, I-V curves are obtained for different applied loads, i.e., under controlled mechanical response of the organic layer. Figure 4 illustrates the procedure. For simplicity, only the normal force image of the α-phase is shown as a three-dimensional plot (Figure 4a). Along the fast scan direction the applied voltage is varied between ± 1 V and along the slow scan direction the sample moves 15 nm towards the tip (from top to bottom in (a)). The approach travel range was chosen to ensure no SAM deformation or indentation. The vertical profile at V = 0 in the force image, $F_n(0, z)$, is presented in Figure 4b. This F-z curve serves to establish the repulsive and attractive interaction regimes during the tip-sample approach. The tip is initially out of contact (starting position, z = 0) and there is no cantilever deflection up to a travel distance of $z \approx 3.5$ nm where a sudden drop of the force indicates that the tip jumps into contact with the SAM surface. Beyond this point, the force increases linearly. Three

representative points have been marked in this part of the F-z curve by different colors. F_n increases with z during the attractive regime (red point) and changes after crossing the zero load point (green dot) to the repulsive regime (e.g. dark blue dot) at z ≈ 11 nm. The $F_n(V, z)$ corresponding to the β-phase (not shown) was similar to that of the α-phase, with the same F-z slope and only a small variation of ≈ 0.1 nN in the adhesion force. In both cases the linear response indicated no film deformation under the force range employed.

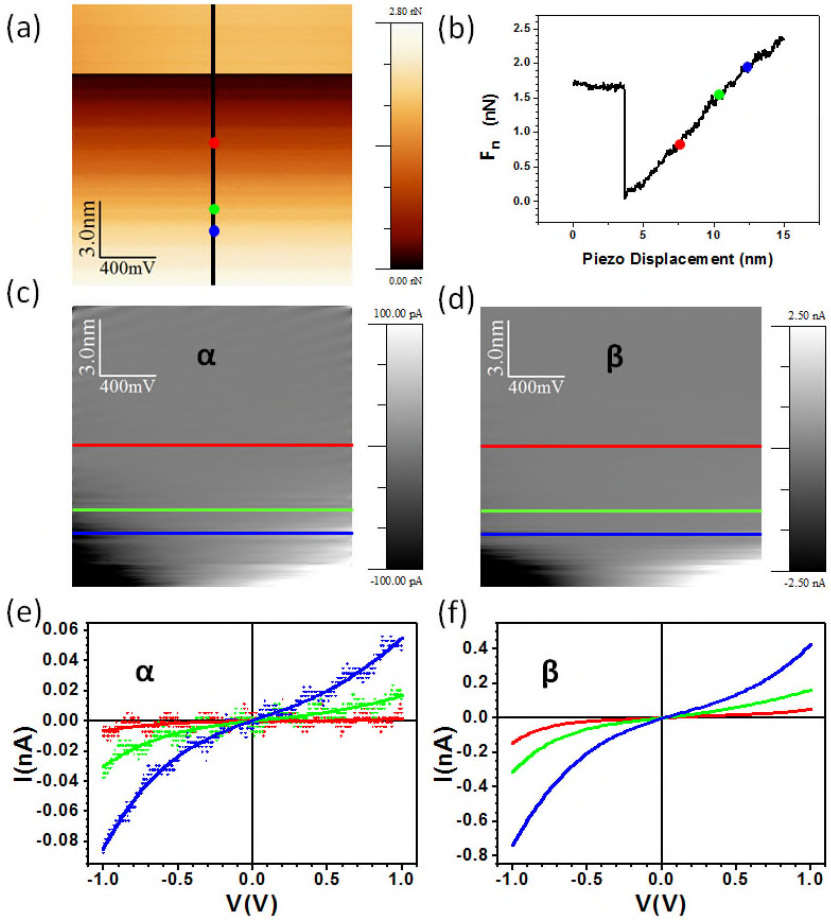

Figure 4. (a) 3D mode normal force image, $F_n(V, z)$, acquired on top of the α-phase. Voltage range is ±1V and total piezo displacement is 15 nm. (b) F-z curve corresponding to the $F_n(0,z)$ line indicated in (a). (c) and (d) Current images, I(V,z),acquired on the α and β-phases,

respectively. (e) and (f) Selected horizontal line profiles extracted from (c) and (d) at the applied loads indicated by the same colors in (b).

The simultaneous I(V, z) images obtained on top of the α and β-phases are shown in Figures 4c and 4d, respectively. The horizontal profiles in these images are the respective I-V characteristics corresponding to the applied loads obtained from the F-z curve on each molecular layer. Therefore, a straightforward comparison between the conducting responses of the two polymorphic phases is possible by direct comparison of I-V curves for specific applied loads. The small currents measured on the α-phase were close to the detection limit (≈ 10 pA) and, only for clarity and guiding the eye, solid line curves are superimposed to the experimental points (Figure 4e) while just raw current data are given for the β-phase (Figure 4f). The load dependent acquisition of I-V curves stopped long before observing the linear behavior characteristic of the ohmic tip-metal substrate contact, thus, guaranteeing no tip penetration into the films.[40]

Commonly, I-V curves of SAMs measured by either STM or C-AFM lead to sigmoidal curves,[40,45] which including intramolecular and intermolecular paths are interpreted within the tunneling mechanism modeled by Simmons.[56] However, all I-V curves recorded on both BP4 phases, Figure 4 (e, f), show only a slightly sigmoidal shape. The junction resistance estimated from the linear low bias region (± 0.4 V) was found to be $R_\beta \approx 10^2$ GΩ and $R_\alpha \approx 10^3$ GΩ for β and α, respectively. The ratio $R_\alpha/R_\beta \approx 10$ is in agreement with relative values for similarly tilted SAMs.[1,18] In the analyzed low force regime, the resistance scales as $R \propto F_n^{-2/3}$ (see Figure S3 in Supporting Information) which corresponds to the contact area dependence with load in the elastic regime.[57] The small asymmetry observed for larger voltages can be accounted for by

using the rectification ratio (RR), defined as RR = |I(–V)/I(+V)|, i.e., the absolute value of the quotient between currents for negative and positive voltages.[58] For V = ± 1V, we obtain RR(α) = 1.6 and RR(β) = 1.9. While these asymmetries can be attributed to diverse factors related to the different top and bottom SAM-electrode contacts, the different asymmetry between phases is directly correlated to differences in the arrangement of the BP4 molecules.[18,59] On the one hand, the contact is different at the two electrode-molecule interfaces not only because of differences in materials of top (tip) and bottom (substrate) electrodes but also because the BP4 anchoring end is chemically bonded to the Au substrate whereas its end group is not.[10] On the other hand, the asymmetric chemical structure of the molecule itself, with the alkyl chain and the biphenyl moiety on the respective SAM sides, can play an important role. Firstly, the efficiency of electron injection at each contact should be different and, secondly, transport across the film (intra and intermolecular) is also anticipated to be non-symmetric.[32,33,60] Independent of all these contributions, RR is sufficiently small only in the very near zero region (below ± 400 mV) to permit fitting the complete I-V curves by a Simmons model but excellent fits are obtained in the range of ± 1V when decomposing the curves into negative and positive branches (see details in Supporting Information). The obtained decay constants are $\kappa_\alpha = 0.98 \pm 0.05$ Å^{-1} and $\kappa_\beta = 0.95 \pm 0.05$ Å^{-1}, for each phase. These values are larger than those corresponding to SAMs of oligophenylene thiols ($\kappa_{Ph} \approx 0.6$-0.7 Å^{-1})[61,62] but in good accordance with reported values obtained by STM on BP4 SAMs for non-penetration conditions.[60] The difference can be ascribed to the presence of methylene units between the aromatic rings and the sulfur anchoring group, which has been argued to increase the decay constant to a value similar to that of a length-matched saturated aliphatic SAM.[21,63]

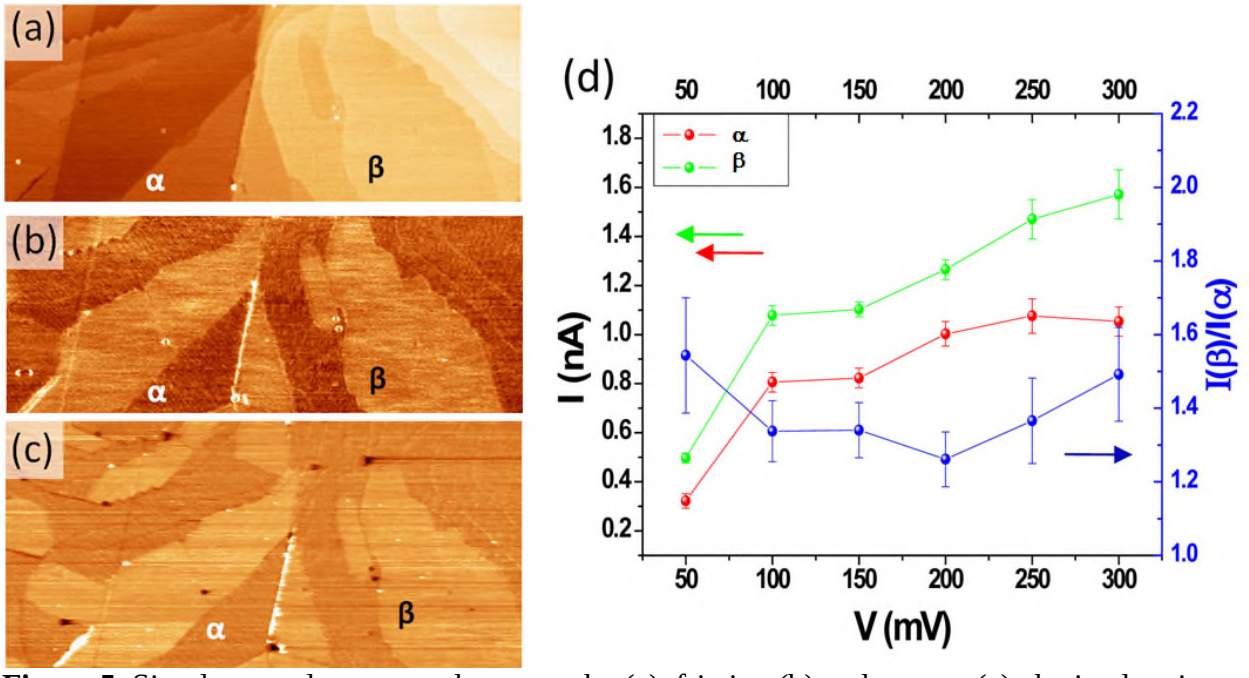

Figure 5. Simultaneously measured topography (a), friction (b) and current (c) obtained at tip-sample voltage V = 100 mV. Lateral x-scan size is 2 μm. Color scale in (c) is 2 nA from black to white. (d) Measured currents and calculated ratios, I(β)/I(α), versus applied voltage.

The local 3D mode employed so far can be extended to maps by exploiting the imaging capability of AFM. Thus, recording all quantities simultaneously, an unequivocal correlation of all signals and comparison between the two phases is established. Figure 5(a-c) presents a complete set of simultaneously recorded topography, friction and current for a given tip-sample bias. The currents documented in Figure 5d were extracted from histograms of the current maps obtained for different bias values (Figure S4 in Supporting Information). As a measure of the precision of the measurements, the error bars in the figure correspond to the standard deviation of the mean (SDOM) estimated from data obtained in more than ten locations for each case. It is worth mentioning that, in order to exclude artifacts due to scan-induced modification, only data

sets with non-changing friction during continuous scanning were used. Interestingly, the ratio I_β/I_α blue in Figure 5d is a rather constant value of about ~ 1.35. By taking into account the molecular density (σ) of each phase ($\sigma_\beta/\sigma_\alpha = A_\alpha/A_\beta \approx 0.83$), the normalized ratio ($|I_\beta/I_\alpha|_{molec}$ ~ 1.6) reveals that the β-phase exhibits a significantly higher conductivity per molecule. This result can be rationalized considering differences between the phases with regard to both the molecular conformation and the SAM/substrate interface. While direct tunneling between electrodes can safely be ignored because such contributions are several orders of magnitude smaller,[18] the pathway of the electronic current flowing through the layers is affected by the structural differences. In fact, a higher current through the β-phase layers ($I_\beta > I_\alpha$) could be explained by the a larger tilt of the molecules in the beta phase. Thus forcing the biphenyl moieties into a more planar conformation a higher conductivity would result compared to a more twisted geometry.[48,49] However, we stress that the magnitude of this effect is unclear as the influence of the SAM-substrate interface, which has been argued to be substantially different for the two phases,[36,37] is not known at present.

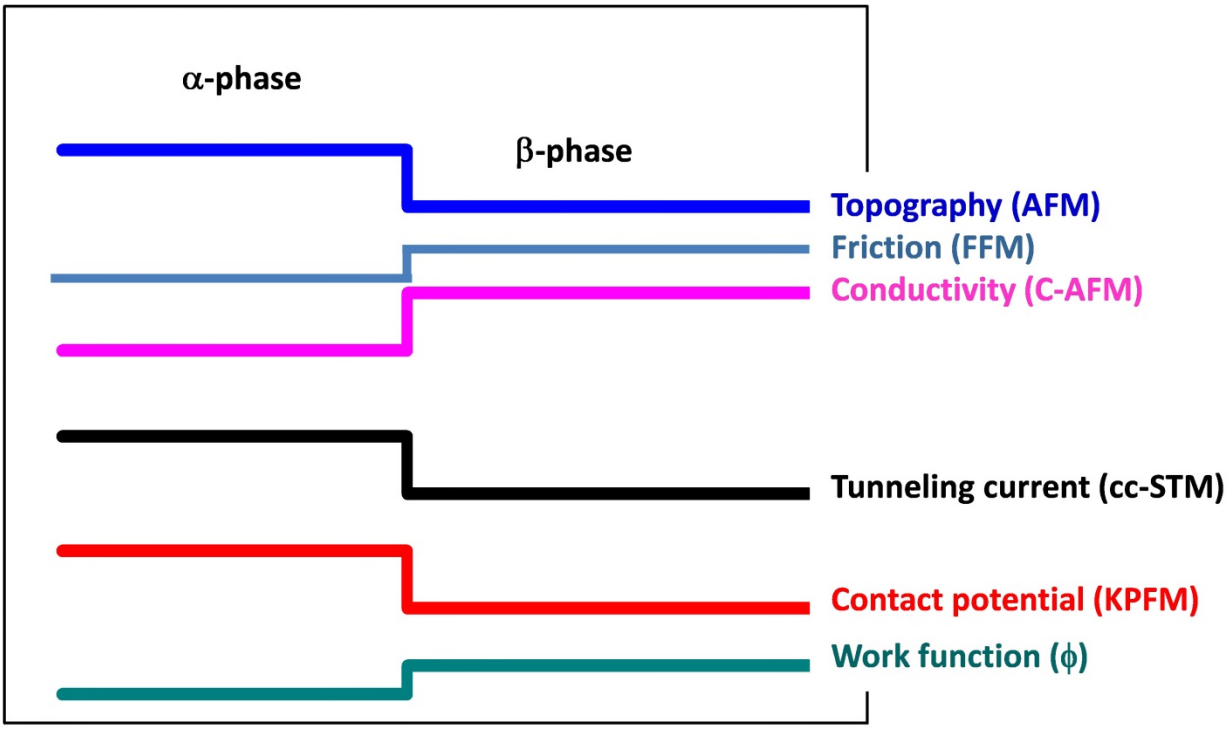

Figure 6. Schematic summary of topography, friction, current, cc-STM, contact potential and work function for the α and β phases of BP4 on Au(111).

As commented above, the transconductance of molecular layers as measured in cc-STM can be understood by using the two-barrier (layer plus vacuum) model in Figure 3. Whereas tunneling through vacuum is described by a typical decay constant of $\kappa_{gap} \approx 2.2$ Å^{-1}, the above presented data provide relative through layer conduction. Since $|I_\beta/I_\alpha|_{molec} \sim 1.6$ a tip retraction on the β-phase compared to the α-phase is expected. Consequently, the measured height difference between the phases is smaller than the geometrical difference in film thickness. By taking into account that in cc-STM the current is kept constant over the whole surface $G_\alpha^{gap} G_\alpha^{SAM} = G_\beta^{gap} G_\beta^{SAM}$ and using the structural data for each polymorph while assuming an average decay constant $\kappa^{SAM} = 0.97$ Å^{-1} for both phases, we obtain a difference in the vacuum gap of $\Delta t = t_\beta - t_\alpha$

≈ 0.5 Å (see Supporting Information) that reconciles the difference of $\Delta h_{STM} - \Delta h_{AFM} \approx 0.4$ Å between the topographic cc-STM and AFM measurements. In summary, although first principle calculations would be essential to completely disentangle all factors in a quantitative manner, competition between barrier heights ($\phi_\alpha < \phi_\beta$) and barrier widths ($d_\alpha > d_\beta$) seems to be balanced by the relative conducting response through each phase ($I_\beta > I_\alpha$). Presenting a qualitative comparison between the different quantities discussed throughout this work, the schematics shown in Figure 6 illustrates their correspondence between the two polymorphic phases.

CONCLUSIONS

The influence of the molecular packing on the functional properties of a biphenyl based thiol SAM has been investigated. This is enabled by the occurrence of two structurally different phases, forming highly crystalline continuous layers, and application of a well-designed combination of AFM modes. Since the molecular building block is identical amongst the two polymorphs, leaving molecular conformation and SAM/substrate interface as the main variables, the relationship between phases and properties is unequivocally established. Besides analyzing the influence of the film structure on the SAM properties, the selected system has been also employed to address the inherent limit of cc-STM for accurately determining topographic differences in the sub-nanometre range between molecular phases coexisting in organic thin films. Considering that coexistence of polymorphs constitutes an ideal scenario for characterization, the presented results are a step forward in the fundamental understanding of structure-property-function correlations in organic layers.

ASSOCIATED CONTENT

Supporting Information. Additional cc-STM and AFM data, including FFM and C-AFM are provided along with details on the employed experimental measuring modes. The following files are available free of charge (pdf).

AUTHOR INFORMATION

Corresponding Author: Carmen Ocal

*E-mail: cocal@icmab.es

Present Addresses

‡Catalan Institute of Nanoscience and Nanotechnology (ICN2), CSIC and BIST, Campus UAB, Bellaterra, 08193 Barcelona, Spain.

§ Instituto de Ciencia de Materiales de Madrid (ICMM-CSIC) Madrid, E-28049, Spain.

Author Contributions

The manuscript was written through contributions of all authors. All authors have given approval to the final version of the manuscript.

ACKNOWLEDGMENT

This work has been supported by the Spanish Government under projects MAT2013-47869-C4-1-P and MAT2016-77852-C2-1-R (AEI/FEDER, UE) and the Generalitat de Catalunya 2014 SGR501. We acknowledge the MINECO project MAT2015-68994-REDC and the ‘‘Severo Ochoa’’ Program for Centers of Excellence in R&D (SEV-2015-0496). M. Paradinas thanks the

Spanish Government for financial support through BES-2008-003588 FPI and PTA2014-09788-I fellowships. C. Munuera thanks financial support from the “Ramón y Cajal” program RYC-2014-16626.

REFERENCES

(1) Salomon, A.; Cahen, D.; Lindsay, S.; Tomfohr, J.; Engelkes, V. B.; Frisbie, C. D. Comparison of Electronic Transport Measurements on Organic Molecules. *Adv. Mater.* **2003**, *15*, 1881–1890.

(2) Solomon, G. C.; Herrmann, C.; Ratner, M. A. Molecular Electronic Junction Transport: Some Pathways and Some Ideas. In *Unimolecular and Supramolecular Electronics II: Chemistry and Physics Meet at Metal-Molecule Interfaces*; Metzger, R. M., Ed.; Springer Berlin Heidelberg: Berlin, Heidelberg, **2012**; pp 1–38.

(3) Ratner, M. Pushing Electrons around. *Nature* **2000**, *404*, 137–138.

(4) Qi, Y.; Liu, X.; Hendriksen, B. L. M.; Navarro, V.; Park, J. Y.; Ratera, I.; Klopp, J. M.; Edder, C.; Himpsel, F. J.; Fréchet, J. M. J.; et al. Influence of Molecular Ordering on Electrical and Friction Properties of ω-(Trans-4-Stilbene) Alkylthiol Self-Assembled Monolayers on Au (111). *Langmuir* **2010**, *26*, 16522–16528.

(5) McCreery, R. L.; Bergren, A. J. Progress with Molecular Electronic Junctions: Meeting Experimental Challenges in Design and Fabrication. *Adv. Mater.* **2009**, *21*, 4303–4322.

(6) Obersteiner, V.; Egger, D. A.; Heimel, G.; Zojer, E. Impact of Collective Electrostatic Effects on Charge Transport through Molecular Monolayers. *J. Phys. Chem. C* **2014**, *118*,

22395–22401.

(7) Chen, F.; Hihath, J.; Huang, Z.; Li, X.; Tao, N. J. Measurement of Single-Molecule Conductance. *Annu. Rev. Phys. Chem.* **2007**, *58*, 535–564.

(8) Brooke, R. J.; Jin, C.; Szumski, D. S.; Nichols, R. J.; Mao, B. W.; Thygesen, K. S.; Schwarzacher, W. Single-Molecule Electrochemical Transistor Utilizing a Nickel-Pyridyl Spinterface. *Nano Lett.* **2015**, *15*, 275–280.

(9) Xie, Z.; Bâldea, I.; Demissie, A. T.; Smith, C. E.; Wu, Y.; Haugstad, G.; Frisbie, C. D. Exceptionally Small Statistical Variations in the Transport Properties of Metal–Molecule–Metal Junctions Composed of 80 Oligophenylene Dithiol Molecules. *J. Am. Chem. Soc.* **2017**, *139*, 5696–5699.

(10) Engelkes, V. B.; Beebe, J. M.; Frisbie, C. D. Length-Dependent Transport in Molecular Junctions Based on SAMs of Alkanethiols and Alkanedithiols: Effect of Metal Work Function and Applied Bias on Tunneling Efficiency and Contact Resistance. *J. Am. Chem. Soc.* **2004**, *126*, 14287–14296.

(11) Kim, B.; Beebe, J. M.; Jun, Y.; Zhu, X. Y.; Frisbie, G. D. Correlation between HOMO Alignment and Contact Resistance in Molecular Junctions: Aromatic Thiols versus Aromatic Isocyanides. *J. Am. Chem. Soc.* **2006**, *128*, 4970–4971.

(12) Halik, M.; Hirsch, A. The Potential of Molecular Self-Assembled Monolayers in Organic Electronic Devices. *Adv. Mater.* **2011**, *23*, 2689–2695.

(13) Hamadani, B. H.; Corley, D. A.; Ciszek, J. W.; Tour, J. M.; Natelson, D. Controlling

Charge Injection in Organic Field-Effect Transistors Using Self-Assembled Monolayers. *Nano Lett.* **2006**, *6*, 1303–1306.

(14) Ma, H.; Yip, H.-L.; Huang, F.; Jen, A. K.-Y. Interface Engineering for Organic Electronics. *Adv. Funct. Mater.* **2010**, *20*, 1371–1388.

(15) Kan, Z.; Colella, L.; Canesi, E. V.; Vorobiev, A.; Skrypnychuk, V.; Terraneo, G.; Barbero, D. R.; Bertarelli, C.; MacKenzie, R. C. I.; Keivanidis, P. E. Charge Transport Control via Polymer Polymorph Modulation in Ternary Organic Photovoltaic Composites. *J. Mater. Chem. A* **2016**, *4*, 1195–1201.

(16) Chung, H.; Diao, Y. Polymorphism as an Emerging Design Strategy for High Performance Organic Electronics. *J. Mater. Chem. C* **2016**, *4*, 3915–3933.

(17) Barrena, E.; Palacios-Lidó, E.; Munuera, C.; Torrelles, X.; Ferrer, S.; Jonas, U.; Salmeron, M.; Ocal, C. The Role of Intermolecular and Molecule-Substrate Interactions in the Stability of Alkanethiol Nonsaturated Phases on Au(111). *J. Am. Chem. Soc.* **2004**, *126*, 385–395.

(18) Frederiksen, T.; Munuera, C.; Ocal, C.; Brandbyge, M.; Paulsson, M.; Sanchez-Portal, D.; Arnau, A. Exploring the Tilt-Angle Dependence of Electron Tunneling across Molecular Junctions of Self-Assembled Alkanethiols. *ACS Nano* **2009**, *3*, 2073–2080.

(19) Munuera, C.; Ocal, C. Load-Free Determination of Film Structure Dependent Tunneling Decay Factors in Molecular Junctions. *J. Phys. Chem. C* **2009**, *113*, 21903–21910.

(20) Ishida, T.; Mizutani, W.; Akiba, U.; Umemura, K.; Inoue, A.; Choi, N.; Fujihira, M.;

Tokumoto, H. Lateral Electrical Conduction in Organic Monolayer. *Society* **1999**, *103*, 1686–1690.

(21) Ishida, T.; Mizutani, W.; Aya, Y.; Ogiso, H.; Sasaki, S.; Tokumoto, H. Electrical Conduction of Conjugated Molecular SAMs Studied by Conductive Atomic Force Microscopy. *J. Phys. Chem. B* **2002**, *106*, 5886–5892.

(22) McCarthy, F. J.; Buck, M.; Hähner, G. Friction and Adhesion on Different Phases of a Biphenyl-Alkanethiol Self-Assembled Monolayer on Gold Studied with Scanning Force Microscopy. *J. Phys. Chem. C* **2008**, *112*, 19465–19469.

(23) Paradinas, M.; Munuera, C.; Silien, C.; Buck, M.; Ocal, C. Heterogeneous Nanotribological Response of Polymorphic Self-Assembled Monolayers Arising from Domain and Phase Dependent Friction. *Phys. Chem. Chem. Phys.* **2013**, *15*, 1302–1309.

(24) Geyer, W.; Stadler, V.; Eck, W.; Zharnikov, M.; Gölzhäuser, A.; Grunze, M. Electron-Induced Crosslinking of Aromatic Self-Assembled Monolayers: Negative Resists for Nanolithography. *Appl. Phys. Lett.* **1999**, *75*, 2401–2403.

(25) Yildirim, C.; Sauter, E.; Terfort, A.; Zharnikov, M. Effect of Electron Irradiation on Electric Transport Properties of Aromatic Self-Assembled Monolayers. *J. Phys. Chem. C* **2017**, *121*, 7355–7364.

(26) She, Z.; DiFalco, A.; Hähner, G.; Buck, M. Electron-Beam Patterned Self-Assembled Monolayers as Templates for Cu Electrodeposition and Lift-Off. *Beilstein J. Nanotechnol.* **2012**, *3*, 101–113.

(27) Creager, S.; Yu, C. J.; Bamdad, C.; O'Connor, S.; MacLean, T.; Lam, E.; Chong, Y.; Olsen, G. T.; Luo, J.; Gozin, M.; et al. Electron Transfer at Electrodes through Conjugated "Molecular Wire" Bridges. *J. Am. Chem. Soc.* **1999**, *121*, 1059–1064.

(28) Sikes, H. D.; Smalley, J. F.; Dudek, S. P.; Chidsey, C. E. D.; Feldberg, S. W. Rapid Electron Tunneling Through Oligophenylenevinylene Bridges. *Science.* **2001**, *291*, 1519–1523.

(29) Silien, C.; Lahaye, D.; Caffio, M.; Schaub, R.; Champness, N. R.; Buck, M. Electrodeposition of Palladium onto a Pyridine-Terminated Self-Assembled Monolayer. *Langmuir* **2011**, *27*, 2567–2574.

(30) Fan, F. R. F.; Yang, J.; Cai, L.; Price, D. W.; Dirk, S. M.; Kosynkin, D. V.; Yao, Y.; Rawlett, A. M.; Tour, J. M.; Bard, A. J. Charge Transport through Self-Assembled Monolayers of Compounds of Interest in Molecular Electronics. *J. Am. Chem. Soc.* **2002**, *124*, 5550–5560.

(31) Adams, D. M.; Brus, L.; Chidsey, C. E. D.; Creager, S.; Creutz, C.; Kagan, C. R.; Kamat, P. V.; Lieberman, M.; Lindsay, S.; Marcus, R. A.; et al. Charge Transfer on the Nanoscale: Current Status. *J. Phys. Chem. B* **2003**, *107*, 6668–6697.

(32) Rong, H. T.; Frey, S.; Yang, Y. J.; Zharnikov, M.; Buck, M.; Wühn, M.; Wöll, C.; Helmchen, G. On the Importance of the Head Group Substrate Bond in Thiol Monolayers: A Study of Biphenyl Based Thiols on Gold and Silver. *Langmuir* **2001**, *17*, 1582–1593.

(33) Cyganik, P.; Buck, M.; Azzam, W.; Wöll, C. Self-Assembled Monolayers of W-Biphenylalkanethiols on Au(111): Influence of Spacer Chain on Molecular Packing. *J.*

Phys. Chem. B **2004**, *108*, 4989–4996.

(34) Shaporenko, A.; Brunnbauer, M.; Terfort, A.; Grunze, M.; Zharnikov, M. Structural Forces in Self-Assembled Monolayers : Terphenyl-Substituted Alkanethiols on Noble Metal Substrates. *J. Phys. Chem. B* **2004**, *108*, 14462–14469.

(35) Dendzik, M.; Terfort, A.; Cyganik, P. Odd − Even Effect in the Polymorphism of Self-Assembled Monolayers of Biphenyl-Substituted Alkaneselenolates on Au (111). *J. Phys. Chem. C* **2012**, *116*, 19535–19542.

(36) Cyganik, P.; Buck, M. Polymorphism in Biphenyl-Based Self-Assembled Monolayers of Thiols. *J. Am. Chem. Soc.* **2004**, *126*, 5960–5961.

(37) Cyganik, P.; Buck, M.; Strunskus, T.; Shaporenko, A.; Wilton-Ely, J. D. E. T.; Zharnikov, M.; Wöll, C. Competition as a Design Concept: Polymorphism in Self-Assembled Monolayers of Biphenyl-Based Thiols. *J. Am. Chem. Soc.* **2006**, *128*, 13868–13878.

(38) Azzam, W.; Cyganik, P.; Witte, G.; Buck, M.; Wöll, C. Pronounced Odd-Even Changes in the Molecular Arrangement and Packing Density of Biphenyl-Based Thiol SAMs: A Combined STM and LEED Study. *Langmuir* **2003**, *19*, 8262–8270.

(39) Horcas, I.; Fernández, R.; Gómez-Rodríguez, J. M.; Colchero, J.; Gómez-Herrero, J.; Baro, A. M. WSXM: A Software for Scanning Probe Microscopy and a Tool for Nanotechnology. *Rev. Sci. Instrum.* **2007**, *78*, 13705–13713.

(40) Munuera, C.; Barrena, E.; Ocal, C. Scanning Force Microscopy Three-Dimensional Modes Applied to Conductivity Measurements through Linear-Chain Organic SAMs.

Nanotechnology **2007**, *18*, 125505.

(41) Paradinas, M.; Garzón, L.; Sánchez, F.; Bachelet, R.; Amabilino, D. B.; Fontcuberta, J.; Ocal, C. Tuning the Local Frictional and Electrostatic Responses of Nanostructured SrTiO3-Surfaces by Self-Assembled Molecular Monolayers. *Phys. Chem. Chem. Phys.* **2010**, *12*, 4452–4458.

(42) Colchero, J.; Storch, A.; Luna, M.; Gómez Herrero, J.; Baró, A. M. Observation of Liquid Neck Formation with Scanning Force Microscopy Techniques. *Langmuir* **1998**, *14*, 2230–2234.

(43) Gómez-Navarro, C.; Gil, A.; Álvarez, M.; Pablo, P. J. De; Moreno-Herrero, F.; Horcas, I.; Fernández-Sánchez, R.; Colchero, J.; Gómez-Herrero, J.; Baró, A. M. Scanning Force Microscopy Three-Dimensional Modes Applied to the Study of the Dielectric Response of Adsorbed DNA Molecules. *Nanotechnology* **2002**, *13*, 314–317.

(44) Crivillers, N.; Munuera, C.; Mas-Torrent, M.; Simão, C.; Bromley, S. T.; Ocal, C.; Rovira, C.; Veciana, J. Dramatic Influence of the Electronic Structure on the Conductivity through Open- and Closed-Shell Molecules. *Adv. Mater.* **2009**, *21*, 1177–1181.

(45) Crivillers, N.; Paradinas, M.; Mas-Torrent, M.; Bromley, S. T.; Rovira, C.; Ocal, C.; Veciana, J. Negative Differential Resistance (NDR) in Similar Molecules with Distinct Redox Behaviour. *Chem. Commun.* **2011**, *47*, 4664–4666.

(46) Heimel, G.; Romaner, L.; Brédas, J.-L.; Zojer, E. Odd-Even Effects in Self-Assembled Monolayers of Omega-(Biphenyl-4-yl)alkanethiols: A First-Principles Study. *Langmuir* **2008**, *24*, 474–482.

(47) Aitchison, H.; Lu, H.; Hogan, S. W. L.; Früchtl, H.; Cebula, I.; Zharnikov, M.; Buck, M. Self-Assembled Monolayers of Oligophenylenecarboxylic Acids on Silver Formed at the Liquid-Solid Interface. *Langmuir* **2016**, *32*, 9397–9409.

(48) Bâldea, I. A Surprising Way to Control the Charge Transport in Molecular Electronics: The Subtle Impact of the Coverage of Self-Assembled Monolayers of Floppy Molecules Adsorbed on Metallic Electrodes. *Faraday Discuss.* **2017**. DOI: 10.1039/C7FD00101K

(49) Mishchenko, A.; Vonlanthen, D.; Meded, V.; Bürkle, M.; Li, C.; Pobelov, I. V.; Bagrets, A.; Viljas, J. K.; Pauly, F.; Evers, F.; et al. Influence of Conformation on Conductance of Biphenyl-Dithiol Single-Molecule Contacts. *Nano Lett.* **2010**, *10*, 156–163.

(50) Duhm, S.; Heimel, G.; Salzmann, I.; Glowatzki, H.; Johnson, R. L.; Vollmer, A.; Rabe, J. P.; Koch, N. Orientation-Dependent Ionization Energies and Interface Dipoles in Ordered Molecular Assemblies. *Nat. Mater.* **2008**, *7*, 326–332.

(51) Miranzo, P.; López-Mir, L.; Román-Manso, B.; Belmonte, M.; Osendi, M. I.; Ocal, C. Prominent Local Transport in Silicon Carbide Composites Containing in-Situ Synthesized Three-Dimensional Graphene Networks. *J. Eur. Ceram. Soc.* **2016**, *36*, 3073–3081.

(52) Aghamohammadi, M.; Fermández, A.; Schmidt, M.; Pérez-Rodríguez, A.; Rodolfo, A.; Fraxedas, J.; Sauthier, G.; Paradinas, M.; Ocal, C.; Barrena, E.; et al. Influence of the Relative Molecular Orientation on Interfacial Charge-Transfer Excitons at Donor/acceptor Nanoscale Heterojunctions. *J. Phys. Chem. C* **2014**, *118*, 14833–14839.

(53) Taylor, D. M.; Bayes, G. F. Calculating the Surface Potential of Unionized Monolayers. *Phys. Rev. E* **1994**, *49*, 1439–1449.

(54) Romaner, L.; Heimel, G.; Ambrosch-Draxl, C.; Zojer, E. The Dielectric Constant of Self-Assembled Monolayers. *Adv. Funct. Mater.* **2008**, *18*, 3999–4006.

(55) Bumm, L. A.; Arnold, J. J.; Dunbar, T. D.; Allara, D. L.; Weiss, P. S. Electron Transfer through Organic Molecules. *J. Phys. Chem. B* **1999**, *103*, 8122–8127.

(56) Simmons, J. G. Generalized Formula for the Electric Tunnel Effect between Similar Electrodes Separated by a Thin Insulating Film. *J. Appl. Phys.* **1963**, *34*, 1793–1803.

(57) Johnson, K. L.; Kendall, K.; Roberts, A. D. Surface Energy and the Contact of Elastic Solids. *Proc. R. Soc. A Math. Phys. Eng. Sci.* **1971**, *324*, 301–313.

(58) Metzger, R. M. Unimolecular Electronics. *J. Mater. Chem.* **2008**, *18*, 4364–4396.

(59) Masillamani, A. M.; Crivillers, N.; Orgiu, E.; Rotzler, J.; Bossert, D.; Thippeswamy, R.; Zharnikov, M.; Mayor, M.; Samorì, P. Multiscale Charge Injection and Transport Properties in Self-Assembled Monolayers of Biphenyl Thiols with Varying Torsion Angles. *Chem. – A Eur. J.* **2012**, *18*, 10335–10347.

(60) Su, G. J.; Aguilar-Sanchez, R.; Li, Z.; Pobelov, I.; Homberger, M.; Simon, U.; Wandlowski, T. Scanning Tunneling Microscopy and Spectroscopy Studies of 4-Methyl-4′-(N-Mercaptoalkyl)biphenyls on Au(111)-(1×1). *ChemPhysChem* **2007**, *8*, 1037–1048.

(61) Holmlin, R. E.; Ismagilov, R. F.; Haag, R.; Mujica, V.; Ratner, M.; Rampi, M. A.; Whitesides, G. M. Correlating Electron Transport and Molecular Structure in Organic Thin Films. *Angew. Chemie-International Ed.* **2001**, *40*, 2316–2320.

(62) Fracasso, D.; Muglali, M. I.; Rohwerder, M.; Terfort, A.; Chiechi, R. C. Influence of an

Atom in EGaIn/Ga2O3 Tunneling Junctions Comprising Self-Assembled Monolayers. *J. Phys. Chem. C* **2013**, *117*, 11367–11376.

(63) Bowers, C. M.; Rappoport, D.; Baghbanzadeh, M.; Simeone, F. C.; Liao, K. C.; Semenov, S. N.; Zaba, T.; Cyganik, P.; Aspuru-Guzik, A.; Whitesides, G. M. Tunneling across SAMs Containing Oligophenyl Groups. *J. Phys. Chem. C* **2016**, *120*, 11331–11337.

TOC Graphic

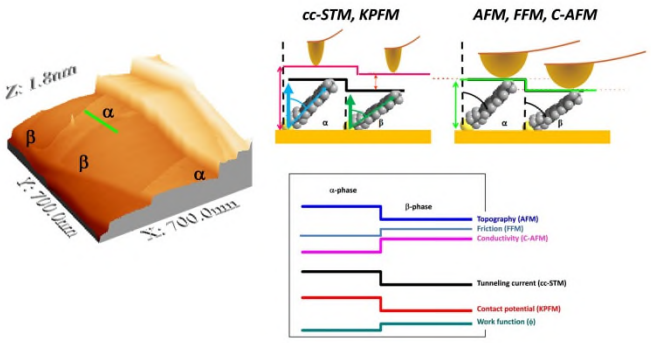
cc-STM, KPFM
AFM, FFM, C-AFM
α
β
β
α
α
β
α
β
α-phase
β-phase
Topography (AFM)
Friction (FFM)
Conductivity (C-AFM)
Tunneling current (cc-STM)
Contact potential (KPFM)
Work function (ϕ)